

Classification Scheme.

## Calculation and Measurements of the Transverse Wake due to Beamline Collimators.

S. Molloy,\* R. Arnold, D. McCormick, Z. Szalata, and M. Woods  
*Stanford Linear Accelerator Center,  
 Menlo Park, CA94025, USA.*

M.W. Slater, N.K. Watson  
*University of Birmingham,  
 Birmingham, UK.*

C.D. Beard and J.L. Fernandez-Hernando  
*Daresbury Laboratory,  
 Warrington, UK.*

A. Bungau  
*University of Manchester,  
 Manchester, UK.*

J.D.A. Smith and A. Sopczak  
*University of Lancaster,  
 Lancaster, UK.*

(Dated: November 2, 2009)

We report on measurements of the transverse wakefields induced by collimators with differing characteristics. An apparatus allowing the insertion of different collimator jaws into the path of a beam was installed in End Station A (ESA) in SLAC. Sixteen comparable collimator geometries were designed, including one that would allow easy comparison with previous results, and were installed in this apparatus. Measurements of the beam kick due to the collimator wakefields were made with a beam energy of 28.5 GeV, and beam dimensions of 100 microns vertically and a range of 0.5 to 1.5 mm longitudinally. The trajectory of the beam upstream and downstream of the collimator test apparatus was determined from the outputs of ten BPMs (four upstream and six downstream), thus allowing a measurement of the angular kick imparted to the beam by the collimator under test. The transverse wakefield was inferred from the measured kick. The different aperture designs, data collection and analysis, and initial comparison to theoretical analytic predictions and numerical calculations are presented here.

PACS numbers: Valid PACS appear here  
 Keywords: Suggested keywords

### I. INTRODUCTION

At the International Linear Collider (ILC) [1] it is expected that significant beam halo will be generated in the acceleration and final focus regions. Allowing this charge to traverse the interaction region (IR) will yield negligible luminosity increase, but, if scattered into the detector by the strong fields of the colliding beams, will degrade its resolution, and, possibly, cause damage. For this reason a collimation section is included in the design of the beam delivery system.

The design for this section involves restricting the aperture of the beampipe at various locations in order to halt any particles located far from the core of the bunch. Correct longitudinal positioning of these inserts will lead to

the halo being removed for all betatron phases. These collimators are often flat, allowing separate control of the two transverse dimensions. As well as continuously absorbing a fraction of the power of the beam, the collimators must be designed to withstand a impact by an entire bunch. Typically a long ( $> 20\chi_0$ ) collimator is “shadowed” by a short ( $0.6 - 1.0\chi_0$ ) spoiler, whose purpose is to enlarge the size of the beam through multiple Coulomb scattering prior to absorption by the collimator, thus reducing the incident power density and the likelihood of damage. It is well known that the electromagnetic field of a charged bunch propagating through a metallic beam-pipe with a relativistic velocity may be disrupted by changes in the geometry of the cross-section of that pipe, by the finite resistivity of the surrounding structure, or by imperfections of the surface finish. In certain situations, the fields excited by the head of the bunch may act on the tail, inducing emittance growth, or, in the worst case, break-up of the beam. The fields result-

---

\*Electronic address: smolloy@slac.stanford.edu

ing from the interaction of the beam with the structure surrounding it are typically referred to as “wakefields”.

Since each of the collimators provide a change in the cross-section of the beam-pipe, it is expected that they will generate wakefields, and are therefore an area of potential emittance growth. For this reason it is important to design collimators to minimise the wakefields they will generate, and, therefore, their impact on the beam.

Previous studies show broad agreement between numerically calculated and measured results [2, 3], but have also demonstrated that performing analytical calculations of these fields can be prohibitively complex, even in very simplified cases. In the regime we study in this paper these differ from numerical estimates and experimental measurements by a factor of  $\sim 2 - 3$ .

In order to design suitable collimators for the ILC, a goal has been set of a  $\sim 10\%$  agreement between the measured and predicted transverse wakes. This paper discusses a supplementary experiment to measure the transverse wake generated by a range of different collimators [4], and to show the level of agreement of these measurements with theoretical and simulated results.

## II. THEORY

The rectangular beam-collimator system, shown in figure 1, can be characterized by a parameter  $\alpha = h\theta/\sigma$  [2]. This allows the classification into so-called *diffractive*, *intermediate* and *inductive* regimes, depending on the minimum separation between the collimator jaws (half-gap,  $b$ ), the width in the orthogonal transverse direction ( $h$ ), the angle formed between the longitudinal axis and collimator ( $\theta$ ) and the mean bunch length ( $\sigma_z$ ). The analytic

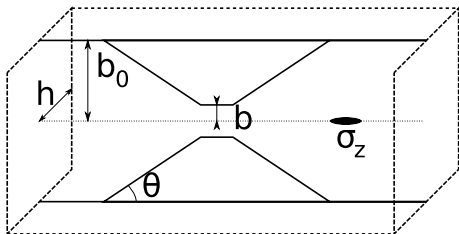


FIG. 1: Diagram illustrating collimator parameters.

calculations of geometric wake which are tested with the T480 data are summarised by [2] for flat collimators in the intermediate and diffractive regimes. Derivations can be found in [5, 6]. The resistive wakefield calculations are based on the study in [7].

While more recent calculations of geometric wakefields in the inductive regime (slowly tapering structures) [8–13] improve the state of the art in the regime that may be required for the ILC, the predicted magnitude of these wakefields is sufficiently small as to be unobservable in the current experiment. Furthermore, only [11] treats the rectangular geometries of interest.

Additionally progress has been made to unite the different regimes for resistive wake calculations, which may enable these to be calculated with more certainty in the future.

There is, nevertheless, some further uncertainty in handling collimators that taper in linearly with two gradients, as shown in figure 2. This geometry is sufficiently complex to be unattainable by existing methods. In these cases we can crudely estimate the kick by calculating the kick contributed by the section between  $r_0$  and  $r_1$ , and add the kick contributed by  $r_1$  to  $r_2$ , though it has been demonstrated [14] that this is not a rigorous treatment. Another method is to avoid effectively double counting the kicks, and just treat the linear taper of the collimator nearest to the beam, effectively bringing in the beam pipe to the radius  $r_1$ . Both treatments have been applied, and in table II we give the results for the latter treatment, the asterisks identify such collimators.

It should be noted that collimator 15, as shown in figure 8 has such a shallow secondary taper, that the diffractive outer section contributes approximately a quarter of the total wake, so neglecting it may give rise to a large error. Additionally, collimator 16 can only be calculated using the formulae for the inductive regime. As these probably do not give an accurate result in the intermediate regime, this has deliberately been excluded from table II.

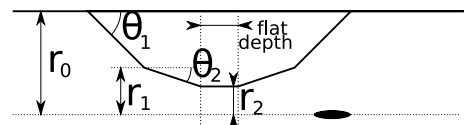


FIG. 2: Diagram illustrating the convention used for numbering collimator jaw parameters.

## III. DESCRIPTION OF EXPERIMENT

Experimental measurements of the collimator kicks were performed at the End Station A (ESA) facility [15] at the Stanford Linear Accelerator Center (SLAC). Transverse wakefields can be measured when a bunch of electrons is passed through a collimator at various offsets from its centre, and it is possible to deduce the scale of the wakefield from the transverse kick received by the bunch.

The ESA facility uses an electron beam extracted from the SLAC linac after acceleration to 28.5 GeV, and steered around a  $24.5^\circ$  bend. There are no magnetic elements in the experimental region of ESA, with the exception of a dipole chicane used in a spectrometry experiment. Table I shows the properties of the ESA beam.

Performing this experiment at ESA yields several advantages:

1. The ESA bunch length and charge are very similar to that proposed for the ILC.

TABLE I: Specifications of the ESA beam.

Beam Property	Value
Charge	$1 - 2 \times 10^{10} e^-$
Energy	28.5 GeV
Repetition rate	10 Hz
Bunch length	0.3 – 1.0 mm
Bunch height $\times$ width	$100 \mu\text{m} \times 1 \text{mm}$

- Since ESA is a facility dedicated to ILC beam-tests, experimenters have control over its operation during their shifts. This means that frequent accesses are possible, and the experimenters have full control over the beam conditions.
- The long bend immediately upstream of ESA allows control over the bunch length in ESA by setting the phase of the accelerating RF in the linac. See table I.
- ESA is equipped with several cranes that facilitate installation of the measurement apparatus (described in subsection III A).

Upstream of the collimator experiment were four RF cavity beam position monitors (BPMs). These were arranged as two doublets; one 44.5 m and one 4 m from the collimator test stand. Downstream were two triplets of cavity BPMs; one 13 m away, and the other 29 m. The trajectory reconstructed from these measurements was used to calculate the kick received from the collimator wakefield.

With an estimated  $1 \mu\text{m}$  uncorrelated, RMS, error on the position measurement from each BPM, the theoretical measurement accuracy of the kick measurement is  $\sim 40 \text{ n-rad}$ . As the downstream BPMs were part of an evolving R&D project, their arrangement was altered for some of the run periods referred to in this paper. The changes, however, were simple rearrangements of the BPMs, as well as the addition of an extra BPM, thus having negligible impact on the theoretical resolution of the wakefield kick measurement.

### A. Collimator Wakefield Apparatus

A so-called “wakefield box” was installed in ESA for the purpose of testing various collimators. This apparatus is detailed in [16], and a schematic is shown in figure 3.

As shown in figure 3, the wakefield box contains an inner “sandwich” in which the collimators to be tested are installed. There are five possible slots through which the beam can move, and four of these are machined to allow installation of collimator jaws. The fifth is left free of obstruction to allow other ESA experiments to run without interruption. A coarse actuator, or “X-mover”,

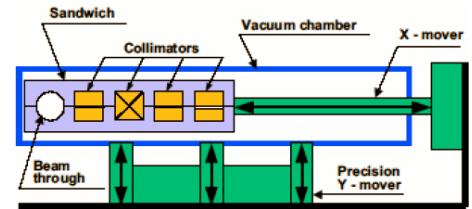


FIG. 3: Schematic of the wakefield collimator box.

is used to move the box to change the slot presented to the beam.

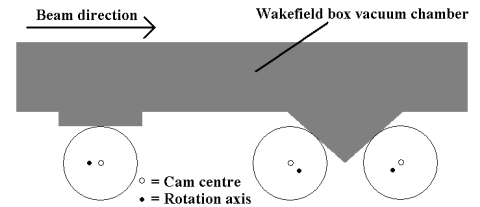


FIG. 4: Cartoon of the cam mover system used to control the wakefield box.

The sandwich is contained within a vacuum chamber, which rests on three motor controlled cams as shown in figure 4. This system of motors allows fine-grained control of the wakefield box in  $y$ ,  $z$ , and  $dy/dz$ , where  $y$  is the vertical axis, and  $z$  is in the direction of beam motion. Full details, including equations of motion, can be found in [17]. For the purposes of this paper it is important to note that this system allows the wakefield box to move  $\pm 1.4 \text{ mm}$  vertically, and that motion in one degree of freedom will reduce the achievable range in the other two. LVDT sensors with a specified resolution of the order of  $1 \mu\text{m}$  were installed at various points on the wakefield box vacuum chamber to provide a readback to the mover control software.

The measurement can proceed by maintaining a steady beam trajectory with position and energy feedbacks, whilst moving the collimator vertically with respect to the beam. This provides more accurate knowledge of the relative offset, and, therefore, the scaling of the wakefield kick with the beam position.

### B. Collimators Tested

The collimators tested in ESA are illustrated in figures 5, 6, 7, and 8. Shown in these figures are the side and beam view of each of the designs, as well as specifications for the half-gap (that is, the distance from the midpoint of the aperture to one of the collimator edges), and the angle of the taper. The differing colours of the sketches in figure 7 distinguish different materials and surface finishes, the details of which are covered in the following text.

The following choices were made in determining the collimator characteristics:

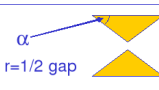
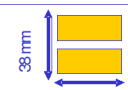




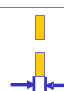

Collim. #	Side view	Beam view	Revised 4-May-2006
1			$\alpha=324\text{mrad}$ $r=2.0\text{mm}$
2			$\alpha=324\text{mrad}$ $r=1.4\text{mm}$
3			$\alpha=324\text{mrad}$ $r=1.4\text{mm}$
4			$\alpha=\pi/2\text{rad}$ $r=4.0\text{mm}$

FIG. 5: Schematic of the collimators from sandwich 1.

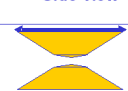







Collim.#	Side view	Beam view	Revised 4-May-2006
8			$r_1=4.0\text{mm}$ $r_2=1.4\text{mm}$ $\alpha_1=289\text{mrad}$ $\alpha_2=166\text{mrad}$
7			$\alpha_1=\pi/2\text{ rad}$ $\alpha_2=166\text{mrad}$ $r_1=4.0\text{mm}$ $r_2=1.4\text{mm}$
6			$\alpha=166\text{mrad}$ $r=1.4\text{mm}$
5			$\alpha=\pi/2\text{rad}$ $r=1.4\text{mm}$

FIG. 6: Schematic of the collimators from sandwich 2.

- Collimator 1

This geometry is identical to one tested in a previous measurement [2], and was included in these tests in order to control systematic errors.

- Collimator 2

This collimator is a linear taper with no additional flat section similar to collimator 1, but with a smaller half gap. It allows the investigation of the dependence on the half gap on the geometric contribution to the kick factor in the ‘intermediate’ regime.

- Collimator 3

This has an identical half gap and taper angle to collimator 2, but with a long flat section, intended to add a large resistive component to the kick. As the length of such a flat section is absent from the most widely used analytical expressions, we can see whether the resistive contribution to the kick factor

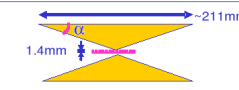
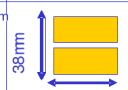
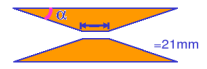

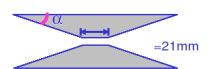

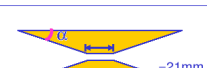

Collim.#	Side view	Beam view	Revised 27-Nov-2006
6			$\alpha=166\text{mrad}$ $r=1.4\text{mm}$ (1/2 gap)
10			$\alpha=166\text{mrad}$ $r=1.4\text{mm}$
11			$\alpha=166\text{mrad}$ $r=1.4\text{mm}$
12			$\alpha=166\text{mrad}$ $r=1.4\text{mm}$

FIG. 7: Schematic of the collimators from sandwich 3.

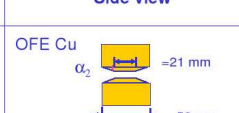
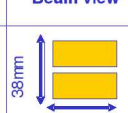
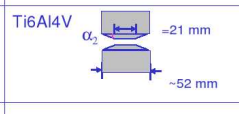

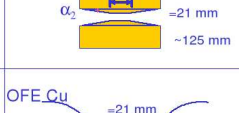



Collim.#	Side view	Beam view	Revised 27-Nov-2006
13			$\alpha_1=\pi/2\text{ rad}$ $\alpha_2=166\text{mrad}$ $r_1=4.0\text{mm}$ $r_2=1.4\text{mm}$
14			$\alpha_1=\pi/2\text{ rad}$ $\alpha_2=166\text{mrad}$ $r_1=4.0\text{mm}$ $r_2=1.4\text{mm}$
15			$\alpha_1=\pi/2\text{ rad}$ $\alpha_2=50\text{mrad}$ $r_1=4.0\text{mm}$ $r_2=1.4\text{mm}$
16			non-linear taper $r=1.4\text{mm}$

FIG. 8: Schematic of the collimators from sandwich 4.

adequately explains the difference between collimators 2 and 3.

- Collimator 4

Step in, step out collimators have been calculated in literature. This example, with 0.5 radiation length thickness allows direct comparison with collimator 5, measuring half-gap dependence in this regime.

- Collimator 5

A diffractive step of 0.5 radiation length thickness allows direct comparison with collimator 4, measuring half-gap dependence in the diffractive regime.

- Collimator 6

This collimators has the same half-gap as collimators 2 and 5, but with a significantly shallower taper angle. Note that this collimator is repeated in figure 7 as it was tested in both series of measurements to ensuring continuity.

- Collimator 7

The two step geometry of collimator 7 is for comparison principally with collimator 4 ( $\pi/2$  taper angle to a half gap of 4 mm), and collimator 6 (identical taper angle at the minimum aperture).

- Collimator 8

Comparison of collimator 8 with collimator 7 enables us to evaluate how much the kick is dominated by the region where the beam travels closest to the collimator.

- Collimator 10

Collimator 10 is like collimator 6 but with an additional flat section, of 0.5 radiation lengths like collimators 11 and 12. It's construction from copper that has been roughened on the surface allows the testing of the dependence of kick factor on surface roughness.

- Collimator 11

Collimator 11 is constructed from a titanium alloy (Ti6Al4V), this can be compared to collimators 10 and 12 to determine the dependence on the resistivity of the collimator material.

- Collimator 12

Equivalent in shape to collimators 10 and 11, collimator 12 allows comparison of the effect of the surface finish, and bulk material properties.

- Collimator 13

Collimator 13 is made with the same taper angle and flat section as collimators 10, 11, and 12, but with an initial  $\pi/2$  step, to further investigate the effect of a sharp change of geometry. Some comparison with collimator 7 can be made, which is similar, but lacks the flat section.

- Collimator 14

An identical geometry to collimator 13 was used for collimator 14, however it was constructed from the same titanium alloy as collimator 11.

- Collimator 15

The shallowest taper angle near the beam of all the collimators was used for collimator 15. Apart from this it is much like collimator 13 in material and shape. Comparison with collimator 6 is very interesting, as it is both shorter and potentially causes less wake.

- Collimator 16

While calculations have been performed in the far inductive regime to determine 'optimal' collimator geometries, such calculations have not been performed in the intermediate regime. The design of collimator 16 considers matching the characteristic impedance of the beampipe as well as possible in a

reasonable distance, and was selected from a collection of geometries with curved profiles. Such profiles are awkward to simulate in numerical packages and demonstrate the advantages of fully conformal techniques. Analytical calculations for such a collimator are difficult in the intermediate regime, so this tests the ability of state of the art numerical calculation.

## IV. SIMULATIONS

### A. Choice of Codes for the Solution of Collimator Wakefield Kicks

Over the last three years there have been significant advances in the tools available for calculation of collimator kicks in three spatial dimensions. In [18] we reported on the use of MAFIA for solving such problems, and while this was somewhat effective for short step collimators, it was clear that a standard desktop PC was unable to solve these problems in 3D. An earlier 'state of the art' for collimator calculations is described in [19].

It was clear that if we used standard finite difference time domain methods we would find ourselves with problems of a size only large clusters and supercomputers could handle. Thankfully, a number of codes have appeared that implement 'moving mesh' algorithms. Amongst those are the code we used for the greater part of our study, GdfidL. Moving mesh, or 'window wake' calculations are also possible with PBCI and ECHO. Both PBCI and ECHO feature algorithms to make the calculations non-dispersive, which reduces numerical noise in the results. Moderately short bunches can also be calculated with recent versions CST particle studio, however without a window wake or parallel running it suffers the same problems as MAFIA, and cannot yet handle short bunch lengths. We will report on those results too. Tau 3P, VORPAL, MEEP and NEKCEM also do not have a moving mesh, and while parallel calculations can be performed with these codes too, it is thought that ECHO, GdfidL and PBCI are currently the most appropriate for this type of calculation. CST Particle Studio claims to handle resistive wall wakes in the same calculations. We restrict ourselves to geometric wake only calculations, leaving the inclusion of resistive effects in numerical codes as future work.

### B. T480 Calculations

At the T480 experiment at SLAC the collimators had twelve distinct geometries. Calculations of the transverse loss as well as kick factor were produced at a variety of different offsets in order to understand the higher order mode dependence. While the collimators are designed to aid understanding of requirements with an ILC bunch length of 0.3 mm, we have chosen to concentrate largely

on 0.5 mm and 1 mm bunch lengths, as these correspond more closely with the ESA beam available at SLAC. For each collimator, bunch length, and offset a resolution convergence was performed, using a procedure described separately by the authors allowing an estimate of uncertainty to be made [20].

The results from these calculations are shown in table II.

example plot of analytic transverse wake potential, GdfidL wake, PBCI wake

For each of 12 geometries show Experimental, GdfidL 500/1000 results overlapping? I think these images

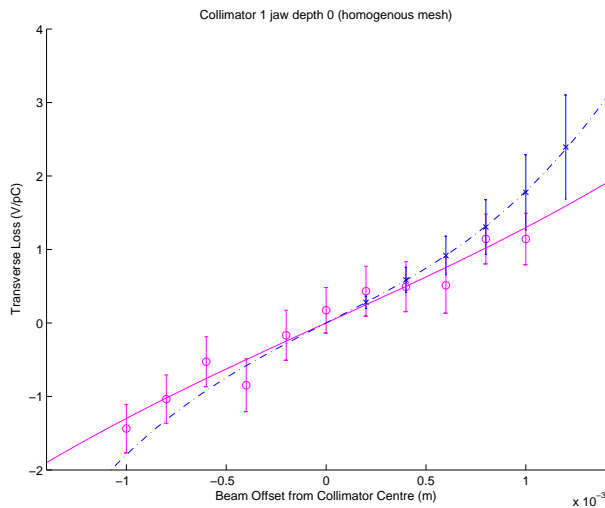


FIG. 9: Experimental and calculated loss factors for collimator 1.

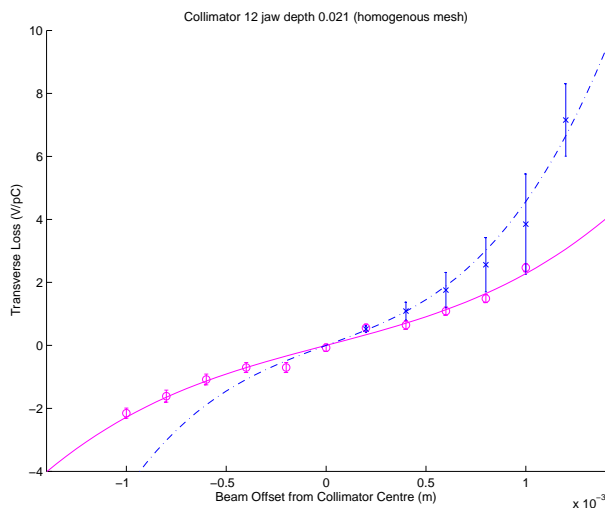


FIG. 10: Experimental and calculated loss factors for collimator 12.

would be better combined into a single figure. Maybe we should include plots for all 12 geometries, or all 16 collimators. Discuss... We can see that in many cases the loss factor calculated in GdfidL bares close resemblance

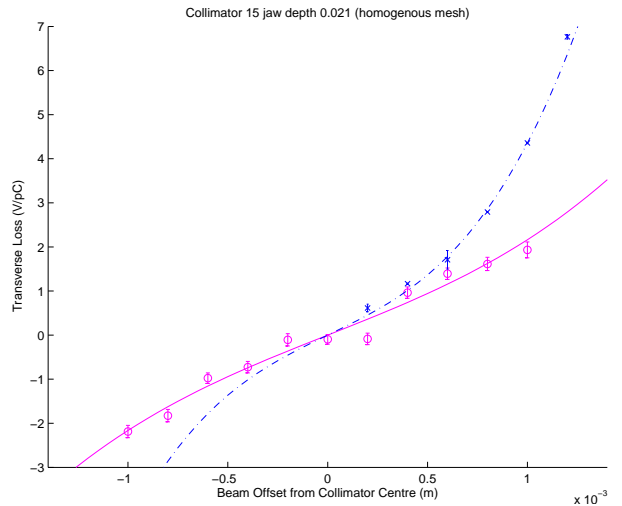


FIG. 11: Experimental and calculated loss factors for collimator 15.

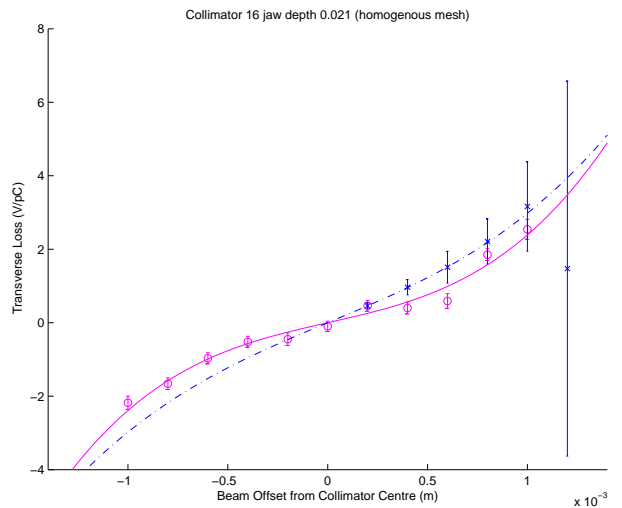


FIG. 12: Experimental and calculated loss factors for collimator 16.

to that observed in experiment, however the calculated value contains neither resistive or surface wall wake effects, and there remains uncertainty in bunch length. [21](reference George & Victoria's paper if it's out in time?)

Explain which results show good agreement, explanation for those that don't. \*\* Placeholder with existing results from Old GdfidL?? Expected accuracy

Discuss future work on entire assembly?

## V. MEASUREMENTS

These collimators were measured over a series of run periods that extended over approximately two years. Due to the large time period between each of these runs, there

TABLE II: Calculated Transverse Geometric Kick Factors for ESA T480 Collimators

Collimator	Analytic (Geometric only)	GdfidL (0.5 mm)	GdfidL (1 mm)	ECHO 3D (0.5 mm)	PBCI (0.5 mm)
1	2.246	1.39 ± 0.29		1.7	
2	5.894	3.06 ± 0.02		3.1	
3	5.894	5.57±		5.1	
4	0.561	0.78±		0.77	
5	4.584	6.07±		6.8	
6,9	4.219	1.64±		2.3	
7	4.244*	2.80±		2.7	
8	4.219*	2.62±		2.4	
10,11,12	4.219	±			
13,14	4.219*	±			
15	2.315 *	±			
16		±			

was a danger of systematic differences in the experiment biasing the results. In order to defend against this possibility, the selection of collimators tested during each run period included at least one that had been measured previously, causing systematic differences to be readily apparent.

As shown in figure 3, it was possible to install four collimators on the beamline for testing. A typical shift would involve presenting each collimator in turn to the beam, and causing the beam to pass through the collimator jaws at a range of vertical positions. This would be repeated several times with the nominal beam parameters in order to gather statistics, and also at multiple bunch lengths and charges in order to confirm the expected scaling with these parameters.

The transverse position of the beam was controlled by a feedback, however there was expected to be a scale error between the step sizes given to the position feedbacks and the actual step of the beam position. Vertical stepper motors on the wakefield box (described in section III A) were expected to be significantly more accurate than the beam feedbacks, so it was decided to hold the beam in the centre of the jaws using these feedbacks, and move the collimators around it.

First the beam feedbacks were tweaked in order to place the beam at the approximate centre of the collimator jaws. To do this, the jaws were scanned in both directions in order to find the point at which significant beam scraping occurred. The feedbacks were then adjusted in such a way that the range of motion upwards was approximately equal to the downward range. This method found the centre with an accuracy of  $\sim 100 \mu\text{m}$  (roughly the vertical size of the bunch).

How the measurements were done. Different charges, and bunch lengths.....

## VI. DATA ANALYSIS

### A. Bunch Length

As detailed in section IV, the wakefield kick is sensitive to the length of the bunch, so it is important that this be controlled and quantified for each of the measurements. The techniques used to measure the bunch length in ESA is detailed in [22], and will be described here briefly.

Due to a lack of suitable diagnostics in ESA it was not possible to perform a direct measurement of this quantity, however since the transfer matrix of the bend is well known, a measurement of the longitudinal phase space of the beam as it enters the bend allows a prediction of the longitudinal phase space in ESA, and, therefore, the expected bunch length.

A CCD screen was used to record an image of the synchrotron radiation emitted by the beam as it moved around the bend. Due to the non-zero dispersion in this region of the machine, the horizontal distribution of this image gives the energy distribution of the bunch.

A transverse cavity at the end of the linac was phased so that the zero crossing of the RF coincided with the longitudinal centre of the bunch. This results in the electrons being given a transverse (vertical) kick, whose amplitude is, to first order, proportional to their longitudinal position within the bunch.

Thus the synchrotron light image contains an expansion of both longitudinal coordinates, and, after calibration of this system, allows extraction of an image of the longitudinal phase space (see figure 13).

$$z_2 = z_1 + R_{56} \cdot \frac{dE}{E} \quad (1)$$

Given the measured profile and the  $R$ -matrix of the bend, it was possible to calculate the expected longitudinal profile in ESA using equation 1, where  $z_i$  is the longitudinal position of each particle ( $i = 1$  indicates the bunch before the bend,  $i = 2$  indicates the bunch after the bend),  $R_{56}$  is the (5, 6) term of the  $R$ -matrix,  $E$  is the

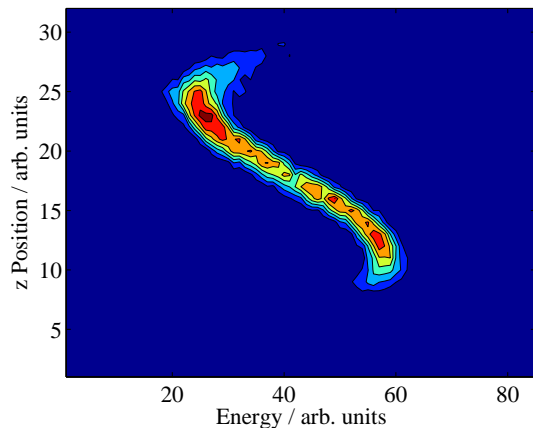


FIG. 13: A digitisation of the synchrotron light image formed at a high dispersion point of the A-line, and with a transverse cavity kicking the beam vertically.

design energy of the bunch, and  $dE$  is the energy error for each particle.

By varying the phase of the accelerating RF in the linac it was possible to obtain a wide range of bunch lengths in ESA (see table I).

Due to the destructive nature of this measurement it was not possible to use it as a continuous measurement of the bunch length. Instead high frequency diodes and a pyro-detector were installed in ESA for this purpose.

These devices are also described in [22]. The basic principle is that a beam will radiate energy if it passes a ceramic gap in the beamline, and the spectrum of this radiation will be a close approximation to the longitudinal profile of the bunch. Therefore, if the radiation is monitored in a frequency band whose wavelength is comparable to the length of the bunch, then any variation in this quantity can be measured. These devices were calibrated against the length extracted from the synchrotron light measurement, and thus provided a non-invasive monitor

of the bunch length in ESA.

Should probably estimate errors on this measurement, but it's been so long..... I have some data-archaeology to do!

## B. Wakefield Kicks

How we extracted the kick factor from the data. Different types of fit. Combining data.

## VII. RESULTS

Theoretical, simulated, and measured results.

Demonstration of consistency of measured results between different data-sets (including PT's). Results from combination of data-sets.

## VIII. DISCUSSION

Discuss the results and do comparison with theory and simulation.

## IX. CONCLUSIONS

Some conclusions. Identify further work.

## Acknowledgments

We wish to acknowledge the support of the operations staff at SLAC, and, . . . .

## APPENDIX A: APPENDIX

- 
- [1] J. Brau et al. (2007), iLC-REPORT-2007-001.
- [2] P. Tenenbaum et al., Phys. Rev. ST Accel. Beams **10**, 034401 (2007).
- [3] P. Tenenbaum, K. Bane, L. Eriksson, R. K. Jobe, D. McCormick, C. Ng, T. O. Raubenheimer, M. C. Ross, G. V. Stupakov, D. Walz, et al., in *Proceedings of the 2001 Particle Accelerator Conference, Chicago* (2001), URL <http://www.slac.stanford.edu/cgi-wrap/getdoc/slac-pub-8937.pdf>.
- [4] O. D., T. O. Raubenheimer, G. V. Stupakov, P. Tenenbaum, and D. Walz, Tech. Rep., Stanford Linear Accelerator Center (2002), URL <http://home.fnal.gov/~onoprien/collwake/nextstage.pdf>.
- [5] G. V. Stupakov, Tech. Rep. SLAC-PUB-7167, Stanford Linear Accelerator Center, Stanford University, Stanford, CA 94309 (1996), URL <http://www.slac.stanford.edu/cgi-wrap/getdoc/slac-pub-7167.pdf>.
- [6] G. V. Stupakov, Tech. Rep. SLAC-PUB-8857, Stanford Linear Accelerator Centre (2001), URL <http://www.slac.stanford.edu/cgi-wrap/getdoc/slac-pub-8857.pdf>.
- [7] P. Tenenbaum and D. Onoprienko, Tech. Rep. SLAC-PUB-10578, SLAC (2004).
- [8] B. Podobedov and S. Krinsky, Physical Review Special Topics - Accelerators and Beams **9**, 054401 (2006), URL <http://prst-ab.aps.org/pdf/PRSTAB/v9/i5/e054401>.
- [9] B. Podobedov and S. Krinsky, Physical Review Special Topics - Accelerators and Beams **10**, 074402 (2007), URL <http://prst-ab.aps.org/pdf/PRSTAB/v10/i7/e074402>.
- [10] B. Podobedov and I. Zagorodnov, in *Proceedings of 2007 Particle Accelerator Conference, Albuquerque, New Mex-*



- ico* (2007), pp. 2006–2008, URL <http://accelconf.web.cern.ch/accelconf/p07/PAPERS/WEOAC04.PDF>.
- [11] G. Stupakov, *Phys. Rev. ST Accel. Beams* **10**, 094401 (2007), URL <http://prst-ab.aps.org/abstract/PRSTAB/v10/i9/e094401>.
- [12] D. A. Burton, D. C. Christie, and R. W. Tucker, in *Proceedings of EPAC08, Genoa, Italy* (2008), URL <http://accelconf.web.cern.ch/AccelConf/e08/papers/tupp026.pdf>.
- [13] D. Burton, D. Christie, J. Smith, and R. Tucker (2009), URL <http://arxiv.org/pdf/0906.0948>.
- [14] I. Zagorodnov and K. Bane, in *Proceedings of 2006 European Particle Accelerator Conference, Edinburgh, UK* (2006), pp. 2859–2861, URL <http://cern.ch/AccelConf/e06/PAPERS/THPCHO36.PDF>.
- [15] M. Woods et al. (2005), physics/0505171.
- [16] P. Tenenbaum et al. (1999), contributed to IEEE Particle Accelerator Conference (PAC 99), New York, NY, 29 Mar - 2 Apr 1999.
- [17] G. Bowden, P. Holik, S. R. Wagner, G. Heimlinger, and R. Settles, *Nucl. Instrum. Meth.* **A368**, 579 (1996).
- [18] C. Beard and J. D. A. Smith, in *Proceedings of 2006 European Particle Accelerator Conference, Edinburgh, UK* (2006), pp. 709–711.
- [19] C.-K. Ng, T. O. Raubenheimer, and P. Tenenbaum, in *Proceedings of the 2001 Particle Accelerator Conference, Chicago* (2001), URL <http://cern.ch/AccelConf/p01/PAPERS/TPPH030.PDF>.
- [20] J. D. A. Smith, EUROTeV MEMO EUROTeV-Memo-2008-004, EUROTeV (2008), URL [http://www.eurotev.org/reports\\_\\_presentations/eurotev\\_memos/e389/e844/infoboxContent42088/EUROTeV-Memo-2008-004.pdf](http://www.eurotev.org/reports__presentations/eurotev_memos/e389/e844/infoboxContent42088/EUROTeV-Memo-2008-004.pdf).
- [21] V. Blackmore, G. Doucas, C. Perry, B. Ottewell, M. F. Kimmitt, M. Woods, S. Molloy, and R. Arnold, *Phys. Rev. ST Accel. Beams* **12**, 032803 (2009).
- [22] S. Molloy et al., in *Proceedings of the 2007 Particle Accelerator Conference, Albuquerque, New Mexico* (2007), contributed to Particle Accelerator Conference, Albuquerque, New Mexico, 25-29 Jun 2007.